Microsc. Microanal. 14, 287–295, 2008
doi:10.1017/S1431927608080380

Microscopy AND Microanalysis

© MICROSCOPY SOCIETY OF AMERICA 2008

Electron Diffraction Based Analysis of Phase Fractions and Texture in Nanocrystalline Thin Films, Part I: Principles

János L. Lábár

Research Institute for Technical Physics and Materials Science, Thin Film Physics Laboratory, H-1121 Budapest, Konkoly-Thege M. út 29-33, Hungary

Abstract: A method for phase analysis, similar to the Rietveld method in X-ray diffraction, was not developed for electron diffraction (ED) in the transmission electron microscope (TEM), mainly due to the dynamic nature of ED. Nowadays, TEM laboratories encounter many thin samples with grain size in the 1–30 nm range, not too far from the kinematic ED conditions. This article describes a method that performs (semi)quantitative phase analysis for nanocrystalline samples from selected area electron diffraction (SAED) patterns. Fractions of the different nanocrystalline components are determined from rotationally symmetric ring patters. Both randomly oriented nanopowders and textured nanopowders, observed from the direction of the texture axis produce such SAED patterns. The textured fraction is determined as a separate component by fitting the spectral components, calculated for the previously identified phases with *a priori* known structures, to the measured distribution. The Blackman correction is applied to the set of kinematic diffraction lines to take into account dynamic effects for medium grain size. Parameters of the peak shapes and the other experimental parameters are refined by exploring the parameter space with the help of the Downhill-SIMPLEX. Part I presents the principles, while future publication of Parts II and III will elaborate on current implementation and will demonstrate its usage by examples, respectively.

Key words: electron diffraction, SAED, ring patterns, nanocrystals, thin films, phase fractions, texture, quantitative analysis, TEM

Introduction

X-ray diffraction (XRD) is one of the most frequently applied methods of structure examinations today. The method of structure analysis and phase analysis from powder diffraction data is well elaborated (David et al., 2002). Its success is based on several factors. One of them is instrumentation. Diffraction peaks can be reproducibly measured with good spectral resolution and with low background. Another element of the success is the processing method. Rietveld not only developed his method to extract quantitative data from the measured X-ray powder diffraction pattern, but also made his computer program public, fostering widespread application of his method (Rietveld, 1969; Young, 1993). Weak interaction of X-rays with matter ensures that X-ray powder diffraction can mainly be regarded as kinematic in nature and only some minor corrections are needed due to extinction effects. Strength of interaction of electrons with matter is much stronger. Although the exact value depends on both the applied wavelengths and the examined materials, as a rule of thumb we can state that the interaction for the electrons of the transmission electron microscope (TEM) is about four to five orders of magnitude stronger than for the X-rays in the usual XRD equipment. Consequently, many of the electron diffraction (ED) patterns are dynamic to some degree. For sample thicknesses that somewhat exceed the dynamic limit,[1] the Blackman correction can be applied (Blackman, 1939). The Blackman correction can equally be applied to single crystalline, mosaic, or polycrystalline samples, whether they are randomly oriented or textured or not. For systematic reflections (simultaneously excited multiple orders of the same reflection), a slight further correction of the potential (introduction of the Bethe potential (Bethe, 1928)) in the Blackman formula must also be considered.[2] For much

Received December 12, 2007; accepted April 8, 2008
*Corresponding author. E-mail: labar@mfa.kfki.hu

[1]The exact value of thickness when dynamic diffraction significantly deviates from the kinematic value depends on both structure and orientation. As an example, Zuo et al. (1993) examined TiAl at 120 kV near the [5,3,−10] zone. They found that kinematic and dynamic intensities deviated by about 10% at 5 nm thickness. The higher the accelerating voltage, the larger thickness produces the same deviation between kinematic and dynamic intensities. (Most TEMs use 200–400 keV today.)

[2]It was also shown in Zuo et al. (1993) that in the mentioned example the deviation of the Bethe-corrected two-beam result from the kinematic value reached about 10% at a thickness of 70 nm. The exact value changes with voltage, structure, and orientation.

thicker single crystals, the dynamic effects can only be perfectly described by the many-beam theory (Fujimoto, 1959; Humphreys, 1979), which was successfully applied in practice to solve structures (Vainshtein, 1964). Zuo and Weickenmeier developed a method for automatic beam selection for many beam computations (Zuo & Weickenmeier, 1995). Several generations from the Russian crystallography school used both kinematic and dynamic ED to analyze crystal structures (Vainshtein et al., 1992). However, a general method to fit electron powder diffraction patterns for phase analysis was not available up to now, not even for thin nanocrystalline TEM samples, where dynamic effects are not too strong. The demand for a method (and for a self-contained computer program to implement it) can be pinpointed in the literature. Weirich and coworkers (Weirich et al., 2000, 2002) used ED patterns from nanocrystalline TiO_2, and after integrating the intensities radially, they supplied the data to a Rietveld program (Rodriguez-Carvajal, 2000) to refine the atomic position of the oxygen atoms. Tonejc et al. (2002) used a similar approach. They deduced the circularly integrated ED intensities with the ProcessDiffraction program (Lábár, 2000) and refined it with FULLPROF (Rodriguez-Carvajal, 2000) to obtain the variation of the unit cell distortion with the processing parameters of the nanocrystalline samples. No dynamic correction was applied in any of these publications. The success of these approaches proves that the kinematic approximation is good for the really nanocrystalline samples.

The kinematic approximation was also successfully applied in qualitative phase identification from ED patterns in the TEM (Lábár, 2002; Li, 2004) for powder samples. The kinematic approximation has also been successful in three-dimensional reconstruction of inorganic structures from ED and high-resolution transmission electron microscopy (HRTEM) data measured on single crystals (Zou & Hovmöller, 2006). Precession of the electron beam frequently seems to improve the validity of the kinematic approximation in single crystals (Nicolopoulos et al., 2006). Jansen (2006) also introduced the dynamic approach into structure refinement from ED, measured on single crystals. There still remained the need for simple (semi)quantitative analysis of powder ED data using both kinematic and a simple dynamic approximation. The method in this article addresses that need.

The presence of texture also modifies both the appearance and the intensities in a measured selected area electron diffraction (SAED) pattern. Processing of general textured patterns is performed by Oleynikov et al. (2006). The method in this article is restricted to a special subset of textured patterns, which is the most frequently encountered in the TEM. We analyze ring patterns that are characteristic not only to randomly oriented powders, but also to patterns from textured powders, seen from the axis of the texture. The aim in our method is not simply to index and measure intensities, but also to use these data to determine the fraction of the textured component.

Measured ED patterns also suffer from instrumental distortions, affecting the positions of the individual diffraction spots. This situation is in contrast to that encountered with XRD and is a weakness of ED, unless special lens-less electron diffractometers are used (Vainshtein et al., 1992). There are different approaches in the literature to correct for this distortion. Jansen used a double polynomial for the correction of the positions of single crystal diffraction spots (Jansen, 2006). Belletti et al. (2000) fitted an approximate grid of straight lines to the measured points. An elliptical correction is applied in the ProcessDiffraction program (Lábár, 2000).

The experimental techniques that form the basis of such methods also advanced in the last decade. Early solutions to record the electron intensities linearly over a large dynamic range by a scintillator and photomultiplier were successful (Vainshtein et al., 1992) but tedious (due to the serial recording) and did not become generally applied. Linear recording of electron intensity in a wide dynamic range became daily practice with the usage of Imaging Plates (IP) (information on IP technology: http://www.ditabis.de/iptech/iptech.html) and scientific grade charge-coupled device cameras in the TEMs. Quantitative processing of SAED patterns and HRTEM images became common practice on the basis of these good-quality digitally-recorded electron intensity distributions (Digital Micrograph, Trademark of GATAN, Inc.). Several scientific methods, implemented in the form of computer programs, use these digital pictures or patterns for phase identification, determining crystal orientation or deducing other physical and crystallographic quantities (Walryck & Andruszkiewicz, 1997; Walck & Ruzakowski-Athey, 1998; Belletti et al., 2000; Dimmeler & Schröder, 2000). Other methods (Narayan, 1986; Hart, 2002) extract similar quantities off-line, from data, obtained either manually or by other processing programs (Hovmöller, 1992; Zou et al., 2004). The first versions of the popular[3] ProcessDiffraction program (Lábár, 2000, 2002, 2005; Lábár & Adamik, 2001) processed SAED patterns, but did not perform (semi)-quantitative phase analysis. This article describes a method to determine the volume fraction of both randomly oriented and (specially oriented) textured crystalline phases in a nanocrystalline, thin TEM sample from its SAED pattern and the implementation of that method in the ProcessDiffraction program. Problems, caused by the presence of some amorphous components, are still to be improved in future extensions of the method. Presently, the effect of the amorphous component is mainly eliminated by empirical approximation of the background under the crystalline peaks.

[3] Over 8,000 visits were registered at the download page of the program: http://www.mfa.kfki.hu/~labar/ProcDif.

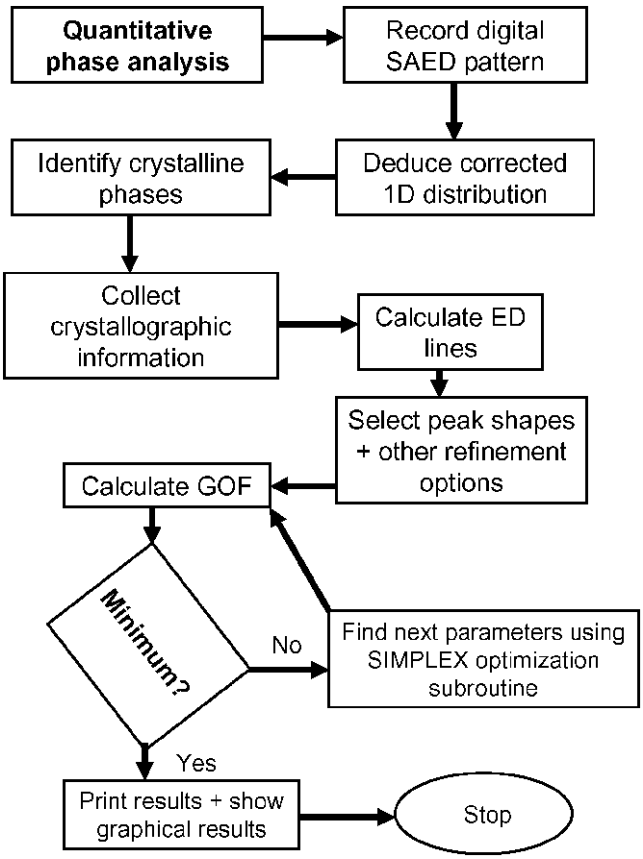

Figure 1. Block diagram, showing the main steps that constitute the method.

Methods

Details of Applied Approaches

Our (semi)quantitative method for phase analysis is based on a few simple steps shown in Figure 1. A typical two-dimensional (2D) SAED pattern is show in Figure 2a. The one-dimensional (1D) distribution deduced from it can be seen in Figure 2b. When the optimized fitting is carried out as shown in Figure 1, the quality of the fit is also to be examined visually. Fitted background and fitted peaks are also indicated in Figure 2b. Occasional false results (systematic deviations of the fitted curve from the measured) can be pinpointed immediately. Strategies and the approximations used during these steps are elaborated below.

Derivation of 1D Intensity Distribution

In contrast to the traditional X-ray power diffraction (e.g., Bragg-Brentano geometry with a point detector); a SAED pattern is a 2D distribution of intensities. In order not to lose information, that 2D distribution is circularly (or more generally elliptically) averaged to obtain an XRD-like 1D distribution, where the intensity is plotted as a function of the length of the scattering vector. For the small scattering angles encountered in SAED of high energy electrons, the length of the scattering vector is almost proportional to the scattering angle (only a minor correction is needed). Correction for a small elliptical distortion (due to the magnetic lenses) is done during this circular (elliptical) averaging, as

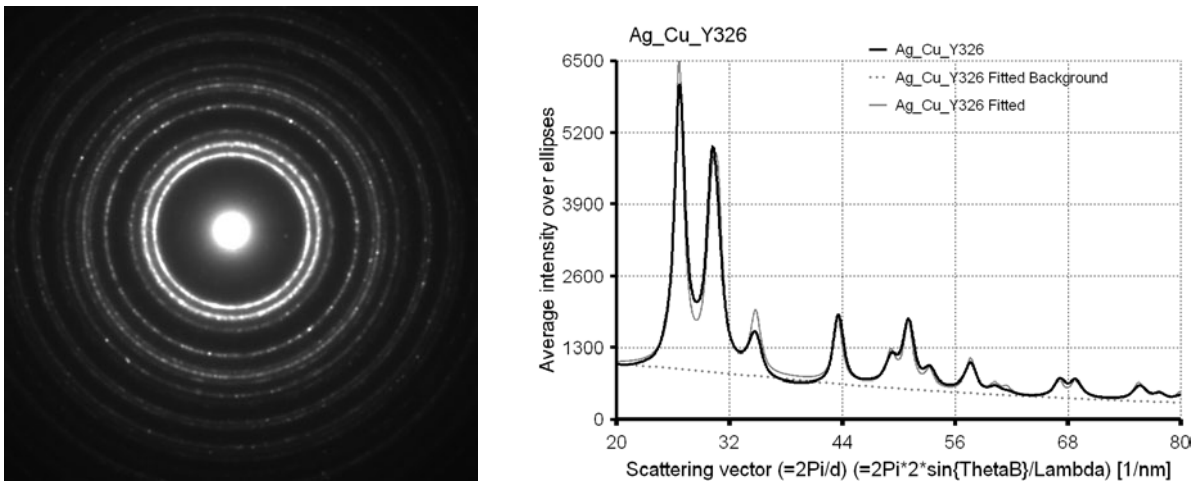

(a) (b)

Figure 2. A typical example: the method is applied here to a test sample, obtained with sequential evaporation of 10 nm Cu and 10 nm Ag on 5 nm amorphous carbon (a-C) film. The self-supporting sample on a Mo-grid was examined at 200 keV in a Philips CM-20 TEM. **a:** The collected 2D SAED pattern. **b:** The 1D distribution obtained from it. 1.5% elliptical correction was detected and corrected for during the derivation of the 1D distribution. The figure also indicates the fitted background and peaks. The log-normal background shape and the Pseudo-Voigt peak-shape were selected for the fit. (Presence of the amorphous component within the background was disregarded.) Fitting resulted in 46 vol% Cu and 54 vol% Ag.

described in the forthcoming Part II of this paper. That distortion is less than 2% for all the TEM SAED patterns encountered by the author.

Identification of Crystalline Phases

A very common situation in analyzing SAED ring patterns is that the list of possible crystalline phases is not know *a priori*; however, the composition of the analyzed volume is known from complementary analysis by either electron energy loss spectroscopy or from X-ray emission spectroscopy (energy dispersive spectrometer). In such situations, the usage of the XRD powder diffraction files is extremely useful because it lists the known phases (that contain the preselected chemical elements) and the positions of their diffraction lines. Although the intensities in the database are strictly valid for XRD only, they also give an estimate of which lines should be strong with electron diffraction, too. The database itself is *not* part of our method; however, legal users of the database can interface to the database from within ProcessDiffraction and use the XRD data as visual Markers aiding phase identification. The interfacing procedure used in the current implementation is elaborated in Part II (forthcoming). All crystalline phases have to be identified prior to the next step of phase analysis.

As described above, the previous tilting experiment should also be used to decide if the identified phase is to be calculated for random orientation, or if a textured version of it is also to be calculated in our method.

Calculation of Marker Data

For qualitative phase identification, or for indexing of single crystal patterns, it is enough to know the positions of the diffracted beams, so XRD data from the power diffraction database can also be used (Lábár, 2002, 2005). However, to quantify the fractions of the phases present, the intensities of the diffracted electrons are also needed. That is why the exact description of the crystal structure of the phases in question must be available. Specification of the structure is performed within a larger crystallography package in ProcessDiffraction, as elaborated in the forthcoming Part II. An important aspect of the implemented crystallographic calculations is that they are placed on a unified platform. In contrast to using individual formulas for each crystal system to calculate spacings of the reflecting planes (d-values in the Bragg equation) and angles between planes and/or between directions, furthermore calculating lengths of real space and reciprocal space vectors, all of these calculations are carried out with the same formulas for all the crystal systems, using the *Metric matrix* and its inverse.

Dynamic Correction

A simple dynamic correction, using the Blackman formula (Blackman, 1939) is also incorporated into our method.

$$\frac{I_{dyn}}{I_{kin}} = \frac{1}{A_h} \int_0^{A_h} J_0(2x) \cdot dx, \tag{1}$$

where $J_0(x)$ is the zero-order Bessel function and $A_h = \sigma \cdot t \cdot |\Phi_h|$, where t is the average grain size in the beam direction (or sample thickness for laterally larger crystallites or single crystals), $\sigma = \pi/\lambda E$ is the coupling constant that relates the amplitude of the scattered wave to the Fourier transform of the potential, and Φ_h is the structure factor for reflection h.

Effect of Precession

There is a strong claim in literature (Berg et al., 1998; Avilov et al., 2007; Oleynikov et al., 2007) that application of a precession camera during the recording of the SAED patterns is frequently efficient in reducing dynamic effects and extending the thickness range where the kinematic approximation is valid. Unfortunately, the author does not have access to such a precession camera at the moment, so testing of the validity of that statement for the case of our method is left for a forthcoming article. That effect would only improve the results obtained with our method, so the message of this article is not affected by the lack of precession.

Temperature Effects

To take the temperature effects into account, the isotropic Debye-Waller factors are incorporated into the method. These factors (and the equivalent average thermal vibration amplitudes) are refined during fitting. Although in principle thermal parameters could be refined independently for each crystallographic site within the asymmetric unit, we only refine a single value for each element present in a given phase. No attempt was made to incorporate the anisotropic vibration ellipsoids (Megaw, 1973).

Textured Powder Patterns

During the Marker-generation step, a texture axis can be specified. The textured Marker will only contain the lines that belong to the zone defined by the texture axis (and its symmetry equivalent directions). These lines consist of a subset of the random Marker lines. Beside the main texture component, a minor texture component(s) can also be defined. Volume fractions of the textured component(s) and the random component are determined simultaneously in the method.

Shapes of Measured Peaks

In contrast to XRD, there are no moving parts and there is no changing solid angle during the recording of the SAED pattern. Furthermore, the recorded range of scattering angles is very much restricted ($<\approx$100 mrad). As a consequence, the dependence of the peak shape and peak width on the scattering angle is much simpler (at least in princi-

ple) than in XRD. However, it is slightly complicated by some additional minor distortions (beam convergence, etc.). To the first approximation, both the shapes and the widths of the peaks belonging to the same phase seem to be constant in a given measurement. The parameters of this shape and width, however, are not known accurately *a priori* for a given instrument but must be calibrated for each measured distribution separately. For XRD, five peak profiles are used for fitting (Snyder, 1993). Three profiles are adapted in the present implementation of the method: Gaussian, Lorentzian, and Pseudo-Voigt, which is a linear combination of the first two. Proportion of the Gaussian component in the Pseudo-Voigt profile can also be refined during parameter optimization. One peak-shape per phase and one peak-width per phase seem to be a good selection in our experience (although several other options are also incorporated in our method). An increased peak-width is an indication of a reduced crystallite size in the nanocrystalline sample; however, other effects, like crystal defects and reflections from the crystallite faces, can also contribute to the broadening. It seems to be unambiguous in XRD (Warren & Averbach, 1950, 1952; Williamson & Hall, 1953; Warren, 1959; Delhez et al., 1993; Cordier et al., 2004), but it is more complicated in the TEM because the recorded peak-width is also affected by the above-mentioned effects.

Background under Peaks

The shape of the background is generally modeled empirically in diffraction experiments (Richardson, 1993). At the present implementation of our method, four shapes can be selected to model the shape of background in 1D SAED distributions: Gaussian (called normal), shifted Gaussian (called log-normal), polynomial and cubic Spline. Log-normal is the default choice because it seems to approximate most of the distributions the best. Apparent deviations from it frequently indicate some problems, such as nonlinear recording or the presence of an amorphous component. It is important to notice that the background is much higher in a SAED pattern of thin nanocrystalline samples than its counterpart in XRD. It is partially connected to the poorer resolution (in Q-space) and partially to the enhanced role of inelastic scattering in SAED. Stray radiation in the microscope may also contribute, but this component should be very small for a good experiment. A polynomial function that is usually applied in XRD (Richardson, 1993) generally does not seem to fit nicely the background in SAED, although it is also offered as an option in our method. Amorphous components are taken into account by either Fourier filtering or by direct modeling in XRD (Richardson, 1993). Within the present version of our method, we included a cubic Spline as an option to try to model the sum of the true background and the amorphous component. It is an empirical option for eliminating the effect of the amorphous component or at least to minimize it.

Optimization of Parameters during Fitting

Parameter optimization tries to minimize the deviation of the entire modeled distribution (background plus all the partial models) from the measured one. To avoid confusion with the special statistical properties of χ^2, we prefer to use a "goodness-of-fit (GOF)" parameter:

$$\mathrm{GOF} = \frac{1}{n-p} \sum_{k=Min-channel}^{Max-channel} \frac{1}{w_k} (Measured_k - Modeled_k)^2, \tag{2}$$

where n is the number of channels and p is the number of parameters to fit.

In the current implementation, w_k is approximated as $Measured_k$. Out of the many possible alternative goodness of fit estimates in use (Young, 1993), our choice corresponds to Young's S^2 definition.

As an additional indicator of good agreement between measured and modeled peak profiles, the Durban-Watson statistics (d_{DW}) is also calculated in our method. Its ideal value is 2.00 (Young, 1993). It measures the correlation between consecutive points in the residuals and is defined as

$$d_{DW} = \frac{\sum_{i=2}^{n} (\Delta y_i - \Delta y_{i-1})^2}{\sum_{i=1}^{n} \Delta y_i^2}. \tag{3}$$

For p parameters to fit, GOF is a function on a p-dimensional space. The task is to find its global minimum. The problem is to avoid deep, local minima. To illustrate the seriousness of the problem, we reproduce Figure 15.1 from Shankland and David (2002) as Figure 3. It shows a 2D section of a 12-dimensional hyper surface, which is calculated while searching for the structure of a molecule from XRD. The flat region of the surface is around $\chi^2 = 1{,}000$, while the deep local minima are approximately $\chi^2 = 200$. It is a strong indication that solution of such problems either requires a very good starting estimate, or the optimization strategy has to have a global character.

In Rietveld refinement by XRD, the initial estimate is rather well known and the closest minimum is generally the global one. "However, in the absence of a well-positioned starting model, standard least-squares refinement simply locates the closest local minimum and terminates at that point" (Shankland & David, 2002, p. 254). The two main classes of global optimization routines are simulated annealing and genetic algorithms, as tersely introduced in Shankland and David (2002). Our selection for optimization is the downhill-SIMPLEX method (Nelder & Mead, 1965), which is a "semiglobal" optimization method, i.e., a local optimizer that looks beyond local minima. Zuo and Spence (1991) also compared different optimization methods while

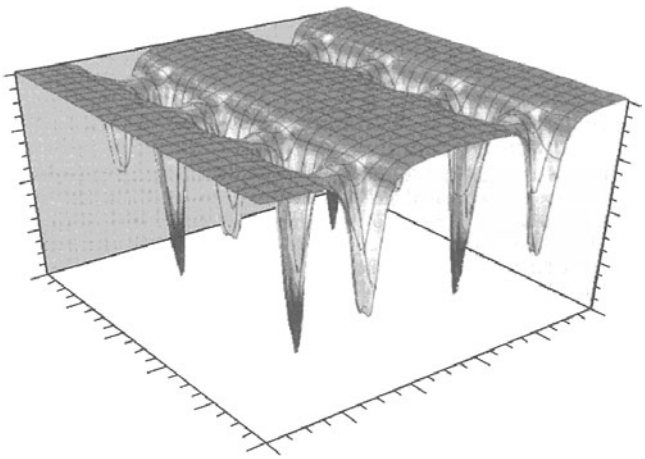

Figure 3. A 2D section of a 12-dimensional hyperspace, showing deep local minima. That hyperspace is explored when the structure of a molecule is determined from its XRD patterns. Reproduced from Figure 15.1 of Shankland and David (2002).

fitting structure factors from CBED. They also found the SIMPLEX method the most robust (Zuo & Spence, 1991; Spence, 1993; Zuo, 1993).[4] Finding the minimum is achieved by going in the direction of the steepest gradient in the multidimensional parameter space with variable step size. As a consequence of this semiglobal nature, each parameter need only be correct half of its parameter space to find the true solution. An important property is that the SIMPLEX only requires function evaluations, not derivatives. It is in contrast to the needs of the Rietveld method. To optimize computational time and to avoid infinite loops, two parameters are specified prior to fitting, the minimal change in the GOF parameter (tolerance) and the maximal number of iteration steps. Restarting the SIMPLEX from the result of a previous fit also increases the chance to escape from a local minimum.

First a "Partial Model" is built up for each crystalline phase, using the parameters, valid in the given iteration step. It is made of the sum of the peaks of that phase in the given fitting interval (calculated using relative line intensities, including texture effects, peak-shapes, and peak-widths). Then the measured 1D diffracted intensity distribution is synthesized as a linear combination of the Partial Models. Because we want the linear combination to be true in all measured channels of the distribution (within the fitting interval) and the number of channels is much larger than the number of phases, the set of equations is very much overdetermined. The usual mathematical method is applied to solve the overdetermined set of equations in a least square sense. The number of equations is reduced, while keeping the information content of all equations by forming matrix $\underline{\underline{a}}$ and vector $\underline{b}$ as

$$a_{i,j} = \sum_k PartialModel_k(i) \cdot PartialModel_k(j),$$

where summation is performed for channels k and

$$b_i = \sum_k (MeasuredDistribution_k - Background_k) \cdot PartialModel_k(i). \quad (4)$$

The coefficients of the linear combination are obtained by solving (for vector $\underline{x}$) the matrix equation:

$$\underline{\underline{a}} \cdot \underline{x} = \underline{b}$$

using matrix inversion.

The coefficients of this linear combination ($x(i)$) place the intensities of the peaks in phase i on an absolute scale. $I_{\max}(i)$, the intensity, calculated on an absolute scale for the strongest (100%) diffraction line of phase i, gives the intensity diffracted by one unit cell (structure factors are calculated for the atoms of one unit cell). Then $x(i)/I_{\max}(i)$ is the number of unit cells of phase i in the analyzed volume. Consequently, the volume extended by phase i in the analyzed volume is $V(i)^*x(i)/I_{\max}(i)$, where $V(i)$ is the volume of the unit cell of phase i. The volume fraction of phase i:

$$Volume\ fraction(i) = \frac{V(i) \cdot x(i)/I_{\max}(i)}{\sum_i V(i) \cdot x(i)/I_{\max}(i)}. \quad (5)$$

The Partial Models are updated in each cycle of the iteration, and the volume fractions are recalculated.

Discussion

Interaction of Parameters

Calibration of the diffracted peak positions is not as accurate for SAED as for XRD. That is because both the exact sample position is difficult to reproduce and the exact position of the recording medium (film, IP) can also change slightly. Slight changes in lens currents also change the camera length. The change in camera length can reach up to 10% (Williams & Carter, 1996), if the condenser currents are changed within the usual limits. All these can be minimized (down to 0.3%) by a careful procedure, but cannot be eliminated completely. That is why camera length is always one of the parameters to refine. Obviously, the same shift can also be actuated by varying the cell parameters of a

[4] In contrast to that observation, Saunders et al. (1995) and Midgley et al. (1995) voted for the usage of the quasi-Newton method.

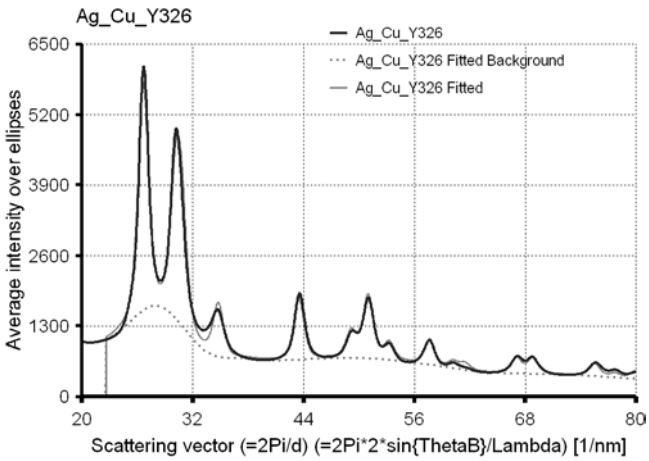

Figure 4. An example of how the presence of an amorphous component in the background is approximated empirically and how the result of the fit is affected. The distribution from Figure 2b is fitted here with the Spline background shape, which is included for empirically taking into account the effect of the amorphous component. Fitting resulted in 51 vol% Cu and 49 vol% Ag.

crystal. Consequently, refinement of all cell parameters is *not* recommended. Refinement of one of some selected cell parameters, however, might be meaningful. For instance, camera length can be set by the majority phase with larger grain size (and consequently sharp peaks), and the distortion in the cell parameters of a minority, very small grained nanocrystalline phase can be refined.

Recorded distributions may also contain some amorphous components. The presence of the amorphous peak (better to say the quality of its approximation in the fitted background) might also interact with the determined peak shape of the overlapping crystalline peaks (see Fig. 4). The present method of Spline fitting to the background takes this effect into account empirically, but it is a limitation to the method through the subjective element in selecting the best background points for fitting. Although the shape is changed conspicuously by the arbitrary approximation of the amorphous component, the resulting phase fractions are only affected within the expected accuracy range of the method. A more accurate method to determine the amorphous component is still to come.

Thermal parameters and the degree of dynamic nature of the reflections also interact. Both of them vary the relative peak intensities of the consecutive diffraction lines of a given phase as a function of the length of the scattering vector (Q). Because the dependence on Q is not identical for these two parameters, they can be distinguished in principle. However, in practice, they may harm each other's accuracy, although the combination of them should provide a good fit and acceptable phase fractions. Consequently, the numerical values of the Debye-Waller factors, determined from SAED, are less reliable than those from XRD.

Both texture and a shift in an atomic position may change the relative line intensities. Refinement of atomic positions should only be attempted on truly random, single phase, very thin nanocrystalline material, without the presence of a disturbing amorphous component. (Possibilities and limitations for refining atomic positions from powder electron diffraction patterns are not discussed in this article. They will form the topic of a forthcoming article.)

Sequence of Refining Parameters

The general approach of the method is to keep control of the stepwise improvement of the parameters by incrementally reducing the tolerance and switching on and off the individual parameters to fit, while visually following the agreement between the fitted and the measured distributions. To facilitate this stepwise improvement, two modes of the fit are offered. One of them reloads all the selected parameters with default values, and Marker data are recalculated from the structure file in order to either start for the first time or to get rid of the results of a previous (probably unsatisfactory) fit. The second mode continues fitting from the results of the previous fit with either a reduced tolerance value or with a parameter set, changed between the two fitting sessions or both. Obviously, if new parameters are switched on for optimization between two such optimization sessions, the new parameters start with default values and only the previously optimized ones keep their previous values. It is also possible to keep previously optimized values for selected parameters (e.g., camera length) but do not vary them further in the consequent sessions (if we find it already accurate enough). Residuals are also shown between the sessions to aid selecting what to change in the optimization setup for the new session.

It is highly recommended that rough manual calibration is performed before entering the quantitative fitting routines. A grossly incorrect starting value for the camera length may lead to an unpredictable, useless result.

Peak-shapes, peak-widths, and camera length are the first parameters to fit (at least to a not too demanding tolerance). Fitting may continue with refinement of thermal parameters and further improvement of peak parameters (improved tolerance). If the camera length has been properly established (with the help of the major phase) and a minor phase seems to have a modified cell parameter (due to distortions in the nanocrystalline state), the camera length may be fixed at the optimized value and (probably one of) the cell parameter(s) of the minor phase can be selected for refinement. However, results of such options (new cell parameters) must be handled even more cautiously than other aspects of the results.

Default values for the individual parameters are estimated prior to the first optimization cycle. These starting estimates are based on the following procedures:

The absolute intensities of the diffracted peaks are automatically estimated from a Wilson-plot (Wilson, 1942).

Integral intensities in preselected intervals of Q are compared to the calculated sum of line intensities in that range. The borders of such intervals are also located automatically, examining minima and maxima in the measured distribution. Because these starting estimates are not too critical for the convergence, no attempt is made here to correct for peak overlaps. This is correctly done in the next cycles.

Starting estimate of peak-widths is deduced from the most intense peak of the given phase. The maximum, close to the nominal peak position, is located, and the minima, closest to it on both flanks, are also identified. A single peak is fitted within the interval between these minima, to the top third of the intensity distribution. In the absence of strong overlaps, that starting estimate is not bad. It is improved quickly in the next cycles of iteration, when the parameter space is explored by the SIMPLEX.

Effect of Energy Filtering

The effect of energy filtering is only to remove the inelastically scattered component. That component mainly influences the (empirically fitted) background, so it is not affecting our phase analysis too much. (That situation is in contrast to that which is experienced during the determination of the short range order from amorphous samples (Lábár et al., 2003).)

Conclusions

A method is presented that can determine both phase fractions and texture (in special patterns) of the nanocrystalline phases present in a thin film sample, measured by electron diffraction in a TEM. The applicable range of grain size (and film thickness) is extended to 10–30 nm by incorporating the Blackman correction for dynamic effects.

Acknowledgments

Financial support of the Hungarian National Research Fund (contract number OTKA T043437) is acknowledged.

References

Avilov, A., Kuligin, K., Nicolopoulos, S., Nickolskiy, M., Boulahya, K., Portillo, J., Lepeshov, G., Sobolev, B., Collette, J.P., Martin, N., Robins, A.C. & Fischione, P. (2007). Precession technique and electron diffractometry as new tools for crystal structure analysis and chemical bonding determination. *Ultramicroscopy* **107**, 431–444.

Belletti, D., Calestani, G., Gemmi, M. & Migliori, A. (2000). QED V1.1: A software package for quantitative electron diffraction data treatment. *Ultramicroscopy* **81**, 57–65.

Berg, B.S., Hansen, V., Midgley, P.A. & Gjonnes, J. (1998). Measurement of three-dimensional intensity data in electron diffraction by the precession technique. *Ultramicroscopy* **74**, 147–157.

Bethe, H.A. (1928). Theorie der Beugung von Elektronen an Kristallen. *Ann Physik* **87**, 55–129.

Blackman, M. (1939). On the intensities of the electron diffraction ring. *Proc Roy Soc London* **A173**, 68–82.

Cordier, P., Ungár, T., Zsoldos, L. & Tichy, G. (2004). Dislocation creep in $MgSiO_3$ perovskite at conditions of the Earth's uppermost lower mantle. *Nature* **428**, 837–840.

David, W.I.F., Shankland, K., McCusker, L.B. & Baerlocher, Ch. (Eds.) (2002). *Structure Determination from Powder Diffraction Data*, IUCr Monographs on Crystallography, No. 13. Oxford: Oxford University Press.

Delhez, R., de Keijser, Th.H., Landford, J.I., Louer, D., Mittemeier, E.J. & Sonneveld, E.J. (1993). Crystal imperfection broadening and peak shape in the Rietveld method. In *The Rietveld Method*, Young, R.A. (Ed.), IUCr Monographs on Crystallography, No. 5, pp. 132–166. Oxford: Oxford University Press.

Dimmeler, E. & Schröder, R.S. (2000). Global least-squares determination of Eulerian angles from single electron diffraction patterns of tilted crystals. *J Appl Crystallogr* **22**, 1088–1101.

Fujimoto, F. (1959). Dynamical theory of electron diffraction in Laue-case, I. General theory. *J Phys Soc Japan* **14**, 1158–1568.

Hart, H.V. (2002). ZONES: A search/match database for single-crystal electron diffraction. *J Appl Crystallogr* **35**, 552–555.

Hovmöller, S. (1992). CRISP: Crystallographic image processing on a personal computer. *Ultramicroscopy* **41**, 121–135.

Humphreys, C.J. (1979). The scattering of fast electrons by crystals. *Rep Prog Phys* **42**, 1825–1887.

Jansen, J. (2006). Structure refinement by taking dynamical diffraction into account. In *Electron Crystallography*, Weirich, Th.E., Lábár, J.L., Zou, X.D. (Eds.), NATO Science Series II: Mathematics, Physics and Chemistry, Vol. 211, pp. 355–372. Dordrecht: Springer.

Lábár, J.L. (2000). ProcessDiffraction: A computer program to process electron diffraction patterns from polycrystalline or amorphous samples. In *Proc. EUREM 12*, Brno, Czech Republic, Frank, L. & Ciampor, F. (Eds.), Vol. III, pp. I379–380. Brno, Czech Republic: Czechslovak Society for Electron Microscopy.

Lábár, J.L. (2002). A tool to help phase identification from electron diffraction powder patterns. *Microsc Anal* **75**, 9–11.

Lábár, J.L. (2005). Consistent indexing of a (set of) SAED pattern(s) with the ProcessDiffraction program. *Ultramicroscopy* **103**, 237–249.

Lábár, J.L. & Adamik, M. (2001). ProcessDiffraction V1.2: New possibilities in manipulating electron diffraction ring patterns. *Microsc Microanal* **7**(Suppl. 2), 372–373.

Lábár, J.L., Kovács, A., Barna, B.P., Hanada, T., Ishimaru, M., Hirotsu, Y. & Bae, I.T. (2003). Variation of the short range order with the composition in an amorphous Al-Pt alloy, existing in a wide compositional range. *Proc. 6th Multinational Congress on Electron Microscopy*, Pula, pp. 469–470. Zagreb, Croatia: Croatian Society for Electron Microscopy.

Li, X.Z. (2004). JECP/PCED—A computer program for simulation of polycrystalline electron diffraction pattern and phase identification. *Ultramicroscopy* **99**, 257–261.

Megaw, H.D. (1973). *Crystal Structures: A Working Approach*. Philadelphia, London, Toronto: W.B. Saunders Company.

Midgley, P.A., Saunders, M., Vincent, R. & Steeds, J.W. (1995). Energy-filtered convergent-beam diffraction: Examples and future prospects. *Ultramicroscopy* **59**, 1–13.

Narayan, C. (1986). A sorting and searching computer program to index electron diffraction patterns from crystals of low symmetry. *J Electron Microsc Tech* **3**, 151–158.

Nelder, J.A. & Mead, R. (1965). A simplex method for function minimization. *Comp J* **7**, 308–313.

Nicolopoulos, S., Kuligin, A., Kuligin, K., Khalid, B., Lepeshov, G., DelPlancke, J.L., Avilov, A., Nickolsky, M. & Ponce, A. (2006). New instrumentation for TEM electron diffraction structure analysis: Electron diffractometry combined with beam precession. In *Electron Crystallography*, Weirich, Th.E., Lábár, J.L. & Zou, X.D. (Eds.), NATO Science Series II: Mathematics, Physics and Chemistry, Vol. 211, pp. 169–184. Dordrecht: Springer.

Oleynikov, P., Hovmöller, S. & Zou, X.D. (2006). Quantification of texture patterns. In *Electron Crystallography*, Weirich, Th.E., Lábár, J.L. & Zou, X.D. (Eds.), NATO Science Series II: Mathematics, Physics and Chemistry, Vol. 211, pp. 121–142. Dordrecht: Springer.

Oleynikov, P., Hovmöller, S. & Zou, X.D. (2007). Precession electron diffraction: Observed and calculated intensities. *Ultramicroscopy* **107**, 523–533.

Richardson, J.W. (1993). Background modeling in Rietveld analysis. In *The Rietveld Method*, Young, R.A. (Ed.), IUCr Monographs on Crystallography, No. 5, pp. 102–110. Oxford: Oxford University Press.

Rietveld, H.M. (1969). A profile refinement method for nuclear and magnetic structures. *J Appl Crystallogr* **2**, 65–71.

Rodriguez-Carvajal, J. (2000). FULLPROF—A Program for Rietveld, Profile Matching and Integrated Intensities Refinement of X-ray and/or Neutron Data. Laboratoire Léon Brillouin, CEA-Saclay, France.

Saunders, M., Bird, D.M., Zaluzec, N.J., Burgess, W.G., Preston, A.R. & Humphreys, C.J. (1995). Measurement of low-order structure factors for silicon from zone-axis CBED patterns. *Ultramicroscopy* **60**, 311–323.

Shankland, K. & David, W.I. (2002). Global optimization strategies. In *Structure Determination from Powder Diffraction Data*, David, W.I.F., Shankland, K., McCusker, L.B. & Baerlocher, Ch. (Eds.), IUCr Monographs on Crystallography, No. 13, pp. 252–285. Oxford: Oxford University Press.

Snyder, R.L. (1993). Analytical profile fitting of X-ray powder diffraction profiles in Rietveld analysis. In *The Rietveld Method*, Young, R.A. (Ed.), IUCr Monographs on Crystallography, No. 5, pp. 111–131. Oxford: Oxford University Press.

Spence, J.C.H. (1993). On the accurate measurement of structure-factor amplitudes and phases by electron diffraction. *Acta Cryst* **A49**, 231–260.

Tonejc, A.M., Djerdj, I. & Tonejc, A. (2002). An analysis of evolution of grain size-lattice parameters dependence in nanocrystalline TiO anatase. *Mater Sci Eng* **C19**, 85–89.

Vainshtein, B.K. (1964). *Structure Analysis by Electron Diffraction*. Oxford: Pergamon Press.

Vainshtein, B.K., Zvyagin, B.B. & Avilov, A.S. (1992). Electron diffraction structure analysis. In *Electron Diffraction Techniques*, Cowley, J.M. (Ed.), IUCr Monographs on Crystallography, No. 3, Vol. 1, pp. 216–312. Oxford: Oxford University Press.

Walck, S.D. & Ruzakowski-Athey, P. (1998). Analysis of selected area diffraction patterns with WINJADE. *Proc Microsc Microanal* **4**.

Walryck, M. & Andruszkiewicz, M. (1997). WINREKS—A computer program for the reciprocal lattice reconstruction from a set of electron diffractograms. In *Electron Crystallography*, Dorset, D.L., et al. (Eds.), pp. 427–430. Dordrecht: Kluwer Academic Publisher.

Warren, B.E. (1959). X-ray studies of deformed metals. *Prog Metal Phys* **8**, 147–201.

Warren, B.E. & Averbach, B.L. (1950). The effect of cold-work distortion on X-ray patterns. *J Appl Phys* **21**, 595–599.

Warren, B.E. & Averbach, B.L. (1952). The separation of cold work distortion and particle size broadening in X-ray patterns. *J Appl Phys* **23**, 497–498.

Weirich, Th.E., Winterer, M., Seifried, S., Hahn, H. & Fuess, H. (2000). Rietveld analysis of electron powder diffraction data from nanocrystalline anatase, TiO_2. *Ultramicroscopy* **81**, 263–270.

Weirich, Th.E., Winterer, M., Seifried, S. & Mayer, J. (2002). Structure of nanocrystalline anatase solved and refined from electron powder data. *Acta Crystallogr* **A58**, 308–315.

Williams, D.B. & Carter, C.B. (1996). *Transmission Electron Microscopy; A Textbook for Materials Science*, p. 285. New York and London: Plenum Press.

Williamson, G.K. & Hall, W.H. (1953). X-ray broadening from filed aluminium and wolfram. *Acta Metallurgica* **1**, 22–31.

Wilson, A.J.C. (1942). Determination of absolute from relative X-ray intensity data. *Nature* **150**, 151–152.

Young, R.A. (Ed.) (1993). *The Rietveld Method*, IUCr Monographs on Crystallography, No. 5. Oxford: Oxford University Press.

Zuo, J.M. (1993). Automated structure-factor refinement from convergent-beam electron diffraction patterns. *Acta Cryst* **A49**, 429–435.

Zuo, J.M & Spence, J.C.H. (1991). Automated structure factor refinement from convergent-beam patterns. *Ultramicroscopy* **35**, 185–196.

Zuo, J.M., Weickenmeier, A.L., Holmstead, R. & Spence, J.C.H. (1993). Are HOLZ lines kinematic in off-zone-axis orientations? In *Proc. 51st Annual Meeting of the Microscopy Society of America*, Bailey, G.W. & Rieder, C.L. (Eds.), pp. 692–693. San Francisco: San Francisco Press.

Zuo, J.M & Weickenmeier, A.L. (1995). On the beam selection and convergence in the Bloch-wave method. *Ultramicroscopy* **57**, 375–383.

Zou, X., Hovmöller, A. & Hovmöller, S. (2004). TRICE—A program for reconstructing 3D reciprocal space and determining unit-cell parameters. *Ultramicroscopy* **98**, 187–193.

Zou, X.D. & Hovmöller, S. (2006). 3D reconstruction of inorganic crystals. In *Electron Crystallography*, Weirich, Th.E., Lábár, J.L. & Zou, X.D. (Eds.), NATO Science Series II: Mathematics, Physics and Chemistry, Vol. 211, pp. 301–320. Dordrecht: Springer.